

Dynamical behavior analysis for small-world scale-free neural networks

Jieyu Lu(鲁婕妤), Jiapeng Ouyang(欧阳佳鹏), Xue Zhao(赵雪), and Minglin Ma(马铭磷)
Citation: Chin. Phys. B, 2026, 35 (**6**): 068708. DOI: 10.1088/1674-1056/ae3609
http://cpb.iphy.ac.cn; http://iopscience.iop.org/cpb

What follows is a list of articles you may be interested in

Bursting synchronization induced by time-delay excitatory or inhibitory autapse in a minimal neuron-astrocyte network

Liao Yu(余廖), Wenlong Zhu(朱文龙), Zhuoqin Yang(杨卓琴), and Zehan Luo (罗泽翰)
Chin. Phys. B, 2026, 35 (**6**): 068705. DOI: 10.1088/1674-1056/ae48c2

Memristor-coupled dynamics and synchronization in two bi-neuron Hopfield neural networks

Fangyuan Li(李芳苑), Haigang Tang(唐海刚), Yunzhen Zhang(张云贞), Bocheng Bao(包伯成), Hany Hassanin, and Lianfa Bai(柏连发)
Chin. Phys. B, 2025, 34 (**12**): 128701. DOI: 10.1088/1674-1056/ae101c

Synchronization and firing mode transition of two neurons in a bilateral auditory system driven by a high-low frequency signal

Charles Omotomide Apata, Yi-Rui Tang(唐浥瑞), Yi-Fan Zhou(周祎凡), Long Jiang(蒋龙), and Qi-Ming Pei(裴启明)
Chin. Phys. B, 2024, 33 (**5**): 058704. DOI: 10.1088/1674-1056/ad1a8e

Dynamical behaviors in discrete memristor-coupled small-world neuronal networks

Jieyu Lu(鲁婕妤), Xiaohua Xie(谢小华), Yaping Lu(卢亚平), Yalian Wu(吴亚联), Chunlai Li(李春来), and Minglin Ma(马铭磷)
Chin. Phys. B, 2024, 33 (**4**): 048701. DOI: 10.1088/1674-1056/ad1483

Dynamical behavior of memristor-coupled heterogeneous discrete neural networks with synaptic crosstalk

Minglin Ma(马铭磷), Kangling Xiong(熊康灵), Zhijun Li(李志军), and Shaobo He(贺少波)
Chin. Phys. B, 2024, 33 (**2**): 028706. DOI: 10.1088/1674-1056/aceee9

SPECIAL TOPIC — Biophysical circuits: Modeling & applications in neuroscience

Dynamical behavior analysis for small-world scale-free neural networks

Jieyu Lu(鲁婕妤)[1], Jiapeng Ouyang(欧阳佳鹏)[1], Xue Zhao(赵雪)[2], and Minglin Ma(马铭磷)[1,†]

[1] *School of Automation and Electronic Information, Xiangtan University, Xiangtan* 411105, *China*
[2] *Xiangtan Central Hospital, Xiangtan* 411105, *China*

(Received 11 November 2025; revised manuscript received 4 January 2026; accepted manuscript online 9 January 2026)

The neural networks of the human brain exhibit dual structural characteristics of small-world and scale-free networks, and their electrical activity is readily modulated by electromagnetic fields. Constructing neural network models that mimic biological structures is crucial for elucidating the brain's information processing mechanisms and the pathological basis of neurological disorders. This paper constructs a small-world scale-free neural network (SWSFNN) model under electromagnetic effects using discrete memristors. By optimizing network topology via graph theory, we systematically investigate how memristor initial values and electromagnetic induction intensity influence the network dynamics. Numerical simulations reveal that memristor initial values affect neuronal firing patterns and regulate network synchronization. We further find a spontaneous "synchronization–cluster synchronization–synchronization" transition under constant parameters. This finding demonstrates that, even in the absence of parameter variations, the inherent nonlinear interactions within the neural network system can drive spontaneous state transitions, thereby generating rich dynamical behaviors. Furthermore, increasing electromagnetic induction intensity also enhances network synchronization. This study provides a theoretical foundation for understanding the nonlinear dynamical mechanisms and synchronization control of neural networks in electromagnetic environments, offering insights for neural computation and information processing.

Keywords: synchronization, electromagnetic effect, small-world characteristics, memristor

PACS: 87.85.dq, 05.45.Xt, 87.19.lj, 05.45.–a

DOI: 10.1088/1674-1056/ae3609 **CSTR:** 32038.14.CPB.ae3609

1. Introduction

In 1971, Professor Chua,[1] starting from the completeness of circuit theory and based on the four fundamental physical quantities — voltage, current, charge, and magnetic flux — hypothesized the existence of a fourth fundamental passive component beyond resistors, capacitors, and inductors. He first proposed the theory of memristors, and this theory was successfully verified experimentally by HP Laboratories in 2008.[2] Owing to its unique nonlinearity and memory characteristics, the memristor exhibits complex dynamical properties within neural networks. Furthermore, its advantages — including nonvolatile storage capability, low power consumption, and high integration density — offer novel research avenues for artificially simulating synapses and constructing brain neural models.[3,4] These properties confer vast application prospects for memristor-coupled neural networks in fields such as the IoT, image encryption, secure communication, and chaotic modeling.[5–9]

Recently, the investigation of neural networks from a physical perspective has garnered increasing attention.[10] This approach motivates the construction of more biophysically plausible models by incorporating elements with clear physical interpretations. For instance, a novel thermosensitive neural circuit was constructed by embedding a thermistor into a memristive FitzHugh–Nagumo model, which successfully mimics the process of perceiving environmental temperature.[11] Extending this physical modeling paradigm, our work focuses on the electromagnetic induction effect in neurons. From a biophysical standpoint, neuronal electrical activity involves the redistribution of ions across the membrane. According to the laws of electromagnetism, these fluctuating ion currents generate time-varying magnetic fields, which in turn induce electromotive forces that feedback to modulate the membrane potential — a phenomenon known as the electromagnetic induction effect. To capture this fundamental coupling between charge and magnetic flux, the flux-controlled memristor provides an ideal mathematical framework. Its distinct physical characteristics allow it to represent electromagnetic effects induced by external electromagnetic fields or internal membrane potentials of neurons, thereby enabling the simulation of neural dynamics in electromagnetic environments.[12] He *et al.*[13] introduced a model named MDW-FOMHNN, which is a fractional-order Hopfield neural network incorporating memristive electromagnetic radiation to produce complex chaotic dynamics. Based on the MDW-FOMHNN, they also designed a straightforward yet effective

[†]Corresponding author. E-mail: minglin_ma@xtu.edu.cn

© 2026 Chinese Physical Society and IOP Publishing Ltd. All rights, including for text and data mining, AI training, and similar technologies, are reserved.

encryption/decryption algorithm, highlighting the immense application potential of memristive electromagnetic phenomena.

To simulate more complex, large-scale networks, research has shifted to the computationally efficient discrete domain. Recently, discrete memristors and maps have gained significant interest owing to their superior efficiency and dynamic richness. Bao *et al.*[14] proposed a general discrete memristor model and constructed discrete memristive hyperchaotic maps, revealing coexisting bi-stable and initial-boosted behaviors. In the context of neural networks, Li *et al.*[15] developed a memristive Rulkov neuron model to investigate magnetic induction effects, identifying complex regime transitions. Furthermore, discrete memristive Hopfield neural networks have been constructed to explore memristor-state-based encryption schemes and heterogeneous neuron dynamics.[16,17] These works provide strong theoretical support for utilizing discrete models to simulate electromagnetic effects in large-scale neural systems.

In memristive neural network research, synchronization, as a typical characteristic, represents the most fundamental mode of neuronal information transmission. It effectively captures neuronal states and patterns within complex neural networks. Most pathological neurological disorders, including epilepsy, tremors, and Parkinson's disease, are intrinsically linked to abnormal neuronal synchronization.[18–21] Muni *et al.*[22] investigated the impact of electromagnetic induction on a ring-star network of Chialvo neurons and discovered the emergence of multiple dynamical regimes, such as chimera states, asynchronous states, and synchronous states. Tang *et al.*[23] proposed a fractional memristive Rulkov neuron model (FMRN), which integrates the fractional discrete HP-type memristor (FDM-HP) into a single fractional Rulkov neuron (FRN). Simulation results indicate that this integration enriches neural system dynamics, enabling synchronous firing rhythms and generating novel firing patterns.

However, past studies on the effects of the electromagnetic environment on neural networks have primarily focused on simple models. On the one hand, higher-level brain functions similarly rely on the collaborative action of neurons and neural clusters across different brain regions. On the other hand, understanding neural network topology is essential in neuroscience research, as the underlying structure of a network also influences the dynamical behaviors of neural systems. Consequently, scholars have shifted their focus to complex neural networks, making them a focus of current research. Complex network theory, grounded in graph theory, integrates methods from statistical physics and nonlinear dynamics. Renowned scientist Qian Xuesen[24] provided a relatively rigorous definition: networks exhibiting some or all of the following properties — self-organization, self-similarity, attractors, small-world characteristics, and scale-free behavior — are termed complex networks. Among these, small-world networks and scale-free networks[25] represent two critically important network architectures within complex networks, attracting extensive attention from researchers.[26–30] Yuan *et al.*[31] proposed a novel small-world neural network using Rulkov neurons, in which the method for determining network coupling strength mimics the construction process of small-world networks, positioning the neural network's coupling strength between randomness and regularity. Deng *et al.*[32] proposed a novel discrete memristive-coupled scale-free neural network. Through dynamical analysis of the initial state, coupling strength, and information transmission delay of memristive synapses, they revealed coexisting neuronal firing patterns and spatiotemporal behaviors including asynchrony, chimera states, synchronization, and synchronization transitions.

Biological experiments based on medical imaging data (e.g., magnetic resonance imaging (MRI), functional magnetic resonance imaging (fMRI), and electroencephalography (EEG)) indicate that brain topology exhibits characteristics of both small-world and scale-free.[33–35] Guo *et al.*[36] employed the Izhikevich neuron model as a basic unit to construct neural networks with several distinct topologies, including random networks, regular networks, small-world networks, scale-free networks, and scale-free networks with small-world properties. They then compared the robustness of neural networks under external noise and found that scale-free networks exhibiting small-world properties demonstrated the greatest robustness to external noise, revealing an intrinsic link between topological structure and functional stability. To more realistically simulate neural networks, it is necessary to consider networks that incorporate multiple properties. Therefore, this study employs discrete memristors to simulate the effects of external electromagnetic fields and constructs a neural network model that combines small-world and scale-free characteristics. The dynamical behaviors of this network are then analyzed from two perspectives: memristor initial values and electromagnetic induction intensity.

The main contributions of this paper are as follows: (i) the construction of a neural network model with small-world and scale-free properties under electromagnetic effects using discrete memristors to simulate external electromagnetic fields; (ii) investigation of the impact of memristor initial values on neural network dynamics; (iii) discovery of a "synchronization–cluster synchronization–synchronization" transition phenomenon under constant parameters; (iv) analysis of the influence of electromagnetic induction intensity on neural network dynamics.

This paper is organized as follows. Section 2 introduces the discrete memristor model, dual-property neural network,

and the proposed SWSFNN model under electromagnetic effects. Section 3 provides a detailed analysis of the network's complex dynamical behaviors from the perspectives of memristor initial values and electromagnetic induction intensity. Section 4 summarizes our conclusions.

2. Construction of SWSFNN under memristive electromagnetic effects

2.1. Discrete memristor model

The discrete memristor used in this study is adopted from Ref. [37], and is described as follows:

$$\begin{cases} i(n) = W((n))v(n) = \varphi(n)v(n), \\ \varphi(n+1) = 0.1f(\varphi) + 0.9\varphi(n) + 0.01v(n), \\ f(\varphi(n)) = \mathrm{sgn}(\varphi(n)) + \mathrm{sgn}(\varphi(n)+2) + \mathrm{sgn}(\varphi(n)-2). \end{cases} \tag{1}$$

Here, $i(n)$ and $v(n)$ represent the current and voltage, respectively. $W(\varphi(n))$ denotes the memristive conductance, where $\varphi(n)$ denotes the discrete memristor's internal state variable. $\varphi(n+1)$ indicates the next state of the memristor, and f is the sign function.

With the initial value set to $\varphi(0) = -1$, a sinusoidal voltage $V = A\sin(2\pi Fn)$ is applied to the discrete memristor. The current–voltage characteristic curve is shown in Fig. 1. These curves exhibit the expected dependencies: Fig. 1(a) illustrates that, at a fixed frequency ($F = 0.1$), the hysteresis loop area increases as the amplitude rises from 2 to 4. Furthermore, Fig. 1(b) demonstrates that the loop area is highly dependent on frequency while holding the amplitude at $A = 5$. As the frequency approaches infinity, the hysteresis loop contracts to a single-valued function. The simulation results demonstrate that the proposed discrete memristor exhibits the fingerprint characteristics of generalized memristors.

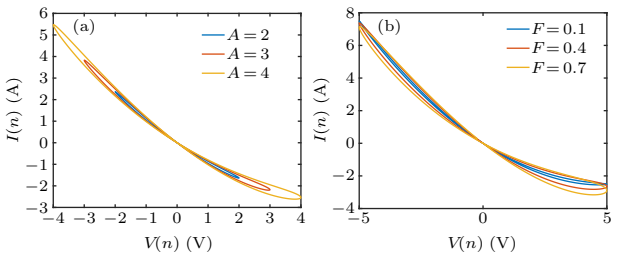


Fig. 1. Fingerprint characteristics of the discrete memristor: (a) At a fixed frequency F, for $A = 2$, 3, and 4. (b) At a fixed amplitude A, for $F = 0.1$, 0.4, and 0.7.

Different initial values can lead to convergence to distinct equilibrium points. Figure 2(a) shows that the discrete memristor settles into four distinct stable states with initial values of -3, -1, 1, or 3, indicating its quadristable characteristic. Based on the multistability analysis shown in Fig. 2(a), the power-off plot (POP) is presented in Fig. 2(b) to further verify the non-volatility of the device. The POP curve exhibits four intersections with the horizontal axis, each with a negative slope. These intersections correspond to the device's stable equilibrium points, thereby providing theoretical support for the device's non-volatile storage capability.

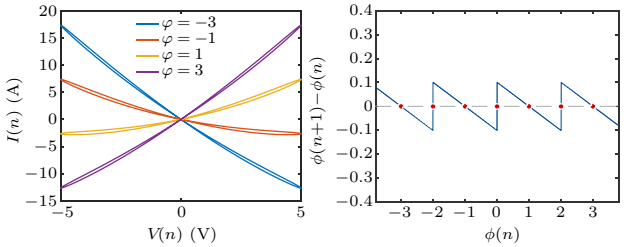


Fig. 2. Physical characteristics of the flux-controlled discrete memristor: (a) Multistability characteristics of the discrete memristor. (b) Power-off plot (POP) for non-volatility analysis.

2.2. Dual-property neural network

The Barrat–Barthélemy–Vespignani (BBV) algorithm generates weighted scale-free networks by combining network growth with the dynamical evolution of link weights.[38] Building upon this foundation, our study employs an improved BBV algorithm to establish a small-world scale-free network with $N = 200$ nodes, which allows the network clustering coefficient to be tuned over a wide range.[39,40] The steps of the algorithm are as follows.

(i) Initial network Initially, a fully connected network with $m_0 = 4$ nodes is generated, yielding an average degree of 3, where all edge weights are initialized to $w_0 = 1$.

(ii) Incorporating a new node With probability p (where $p \in (0, 1]$), a new node u is incorporated into the network. This node connects to three distinct pre-existing nodes, thereby forming three edges. A weight-priority mechanism governs the selection process for these connections. The probability $\Pi_{u\to i}$ of choosing an existing node i is given by

$$\begin{cases} \Pi_{u\to i} = \dfrac{s_i}{\Sigma s_1}, \\ s_i = \displaystyle\sum_{j\in\Gamma(i)} w_{ij}. \end{cases} \tag{2}$$

Here, s_i and w_{ij} denote the node strength and edge weight, respectively. Node i represents an existing node selected for connection by node u, while node j denotes a neighboring node of i. The network generation process is considered complete once the total number of nodes reaches N.

(iii) Incorporating new edges With probability $1 - p$, no new node is added to the network; instead, two new edges are introduced. The creation of each new edge between two existing nodes is governed by a triplet formation mechanism.

First, a random edge $\{a, b\}$ is selected. Subsequently, a third node c is selected from the neighbors of a (subject to $c \neq b$) according to the following weight-priority rule:

$$\Pi_c = \frac{w_{ac}}{(s_a - w_{ab})}. \tag{3}$$

The relationship between nodes c and b is then examined. If they are not connected, a new edge $\{b,c\}$ is established with $w_{bc} = 1$. Simultaneously, the weights w_{ab} and w_{ac} are both incremented by 1. Conversely, if an edge already exists between c and b, the weights w_{bc}, w_{ab}, and w_{ac} are all incremented by 1. The triplet formation mechanism is illustrated in Fig. 3.

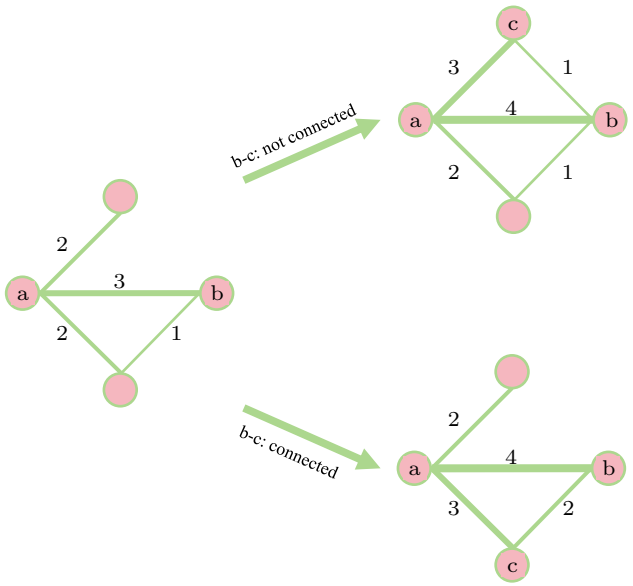


Fig. 3. Mechanism diagram of triplet formation. Pink dots represent neurons; green lines denote inter-neuronal connections. The numbers adjacent to green lines indicate connection weights; larger numbers correspond to thicker lines and stronger connections.

Following these procedures, a weighted small-world scale-free neuronal network (SWSFNN) can be constructed. As the present study only requires consideration of the network topological structure, the weighted network is converted into a binarized network: an edge weight of 1 signifies an existing connection, while an edge weight of 0 signifies its absence. This yields the topological structure of the SWSFNN model.

Different values of p generate networks with distinct topological characteristics, exhibiting varying levels of small-world and scale-free properties, along with other network attributes. The selection of an appropriate p is therefore guided by three key metrics: the average clustering coefficient (ACC), the average shortest path length (ASPL), and the small-world property. The definitions are as follows.

(i) The ACC quantifies the overall connection density of the network. The clustering coefficient of node i measures how closely its neighbors are interconnected, and the ACC is defined as the average of all node clustering coefficients across the network. As an indicator of network compactness, a higher ACC implies tighter connections and greater network cohesion. It is defined by

$$\bar{C} = \frac{1}{N}\sum_{i=1}^{N}\frac{2e_i}{k_i(k_i-1)}, \tag{4}$$

where e_i denotes the number of edges between neighbors of node i, and k_i represents the degree of node i.

(ii) The ASPL measures the efficiency of information transmission in the network. The shortest path length is defined as the minimum number of steps required to travel between any two nodes i and j. The ASPL is computed as the average shortest path length over all pairs of nodes. A lower ASPL indicates more efficient information propagation. It is defined as

$$L = \frac{1}{N(N-1)}\sum_{i\neq j} d_{ij}, \tag{5}$$

where N denotes the total number of nodes in the network, and d_{ij} represents the shortest path length between node i and node j.

(iii) High ACC and low ASPL are fundamental characteristics of small-world networks. To quantify this property, the small-world metric σ is introduced, combining ACC and ASPL. It is defined as

$$\sigma = \frac{C/C_{\text{random}}}{L/L_{\text{random}}}, \tag{6}$$

where C denotes the ACC and L denotes the ASPL of the SWSFNN, while C_{random} and L_{random} correspond to those of a random network with the same size and average degree. A value of $\sigma > 1$ indicates that the network possesses small-world properties, whereas $\sigma \leq 1$ indicates otherwise. A larger σ signifies stronger small-world characteristics. The network topological properties can be tuned via p. The small-world characteristic curves of scale-free networks with different p values are shown in Fig. 4(a).

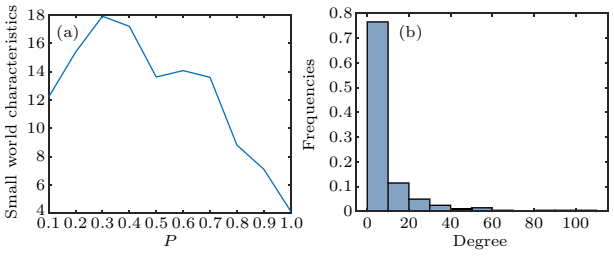


Fig. 4. Topological characteristics of the network. (a) Small-world characteristics σ of the network versus probability p. (b) Degree distribution of the network at $p = 0.3$.

Figure 4(a) clearly demonstrates that the network exhibits the strongest small-world characteristics when $p = 0.3$. To further verify the scale-free property of the constructed network, the degree distribution at $p = 0.3$ is plotted in Fig. 4(b). As shown, the degree distribution follows an approximate power-law distribution, with a small number of highly connected hub nodes. This confirms the scale-free characteristic of the network.[41] Therefore, we select the topology with $p = 0.3$ for subsequent analysis, as it simultaneously exhibits significant small-world and scale-free characteristics.

2.3. SWSFNN model under memristive electromagnetic effects

This study employs the chaotic Rulkov neuron model,[42] whose mathematical expression is given by

$$\begin{cases} x_{n+1} = \dfrac{\alpha}{1+x_n^2} + y_n, \\ y_{n+1} = y_n - b(x_n - \delta), \end{cases} \tag{7}$$

where x and y represent the membrane potential (fast variable) and neuron recovery variable (slow variable), respectively. α and b are control parameters, while δ denotes the external input.

An external electromagnetic field is then modeled using discrete memristors to construct an SWSFNN under electromagnetic effects. The model is given by

$$\begin{cases} x_i(n+1) = \dfrac{\alpha}{1+x_i^2(n)} + y_i(n) + k\sum\limits_j \varepsilon_{ij}(x_j(n) - x_i(n)) \\ \qquad\qquad + w\phi_i(n)x_i(n), \\ y_i(n+1) = y_i(n) - b(x_i(n) - \delta), \\ \phi_i(n+1) = 0.1f(\phi_i(n)) + 0.9\phi_i(n) + 0.01x_i(n), \\ f(\phi_i(n)) = \mathrm{sgn}(\phi_i(n)) + \mathrm{sgn}(\phi_i(n)+2) + \mathrm{sgn}(\phi_i(n)-2), \end{cases} \tag{8}$$

where k denotes the coupling strength, and w represents the magnetic flux feedback intensity. α is a parameter of the Rulkov neuron model, with $\delta = -1$ and $b = 0.001$. ε_{ij} is the connection matrix, where $\varepsilon_{ij} = 1$ indicates a memristive synapse between neurons i and j, and $\varepsilon_{ij} = 0$ otherwise.

3. Analysis of dynamical behaviors in SWSFNN

Abnormal neuronal firing in the brain is closely associated with the onset of numerous neurological disorders. Investigating synchronized firing patterns is crucial for understanding perception, memory, learning, and disease mechanisms. This section investigates the dynamic behaviors of the SWSFNN from the perspectives of memristor initial values and electromagnetic induction intensity.

Numerical simulations are performed using the discrete map in Eq. (8). Each simulation runs for 30000 iterations, and the data shown in figures correspond to the interval $[18000, 28000]$. To systematically reveal different firing patterns, we employ multiple visualization methods — including spatiotemporal patterns, neuron firing diagrams, and instantaneous state plots — to examine how memristor initial values and electromagnetic induction intensity affect network dynamics. In spatiotemporal patterns, the horizontal axis denotes time, the vertical axis denotes neuron index, and the color represents membrane potential x, where brighter colors indicate higher values.

3.1. Effect of memristor initial values on neural network

First, system parameters are fixed at $\alpha = 3.5$, $b = 0.001$, $\delta = -1$, $k = 0.001$, and $w = 0.3$. The initial values of both fast and slow variables are set to 0. We investigate how different memristor initial values affect firing and synchronization behaviors.

When the memristor initial value is -3, Figs. 5(a1)–5(c1) show that the network exhibits no firing activity. When it is -1, Figs. 5(a2)–5(c2) indicate that neurons begin to fire, exhibiting triangular bursting patterns, and the network remains asynchronous. When the memristor initial value is 1, Figs. 5(a3)–5(c3) show triangular bursting with larger amplitudes, and the spatiotemporal patterns become more uniform, indicating improved synchronization. Finally, when the initial value is 2, Fig. 5(a4) shows more complex firing: neurons initially spike and then return to triangular bursting. Figure 5(b4) indicates that the network is nearly synchronized. The instantaneous state at $t = 22500$, shown in Fig. 5(c4), confirms that the network achieves complete synchronization.

In summary, increasing the memristor initial value significantly alters neuronal firing patterns and enhances synchronization, leading the network from asynchrony to complete synchronization in certain intervals.

A closer observation of Fig. 5(a4) reveals that the network does not remain fully synchronized throughout the firing process. Around $t = 22000$, the pattern exhibits alternating structures, suggesting a cluster synchronization state with two distinct membrane potential levels.

To verify this, we plot instantaneous states at $t = 21500$, 22000, and 22500 in Fig. 6. These are representative time points. Figure 6(a) shows complete synchronization at $t = 21500$, corresponding to spiking dynamics. Figure 6(b) shows cluster synchronization at $t = 22000$. By $t = 22500$, as shown in Fig. 6(c), the network returns to a fully synchronized state while the neurons are in a transition from bursting to resting.

Thus, under a fixed memristor initial value of 2 and all other parameters unchanged, the constructed SWSFNN exhibits a remarkable phenomenon: it transitions from complete synchronization to cluster synchronization and back to complete synchronization. As evidenced by the continuous spatiotemporal evolution in Fig. 5(a4), the system evolves smoothly between these regimes without exhibiting intermediate dynamical states. We refer to this behavior as a parameter-invariant "synchronization–cluster synchronization–synchronization" transition. In contrast to previously reported synchronization transitions induced by parameter variation, the transition observed here emerges without any changes in system parameters, representing a novel phenomenon that has not been reported previously. This finding suggests that neural networks possess a richer and more autonomous repertoire of dynamical behaviors than previously understood. Even in the absence of external parametric perturbations, intrinsic nonlinear interactions within the neural system can spontaneously drive such state transitions.

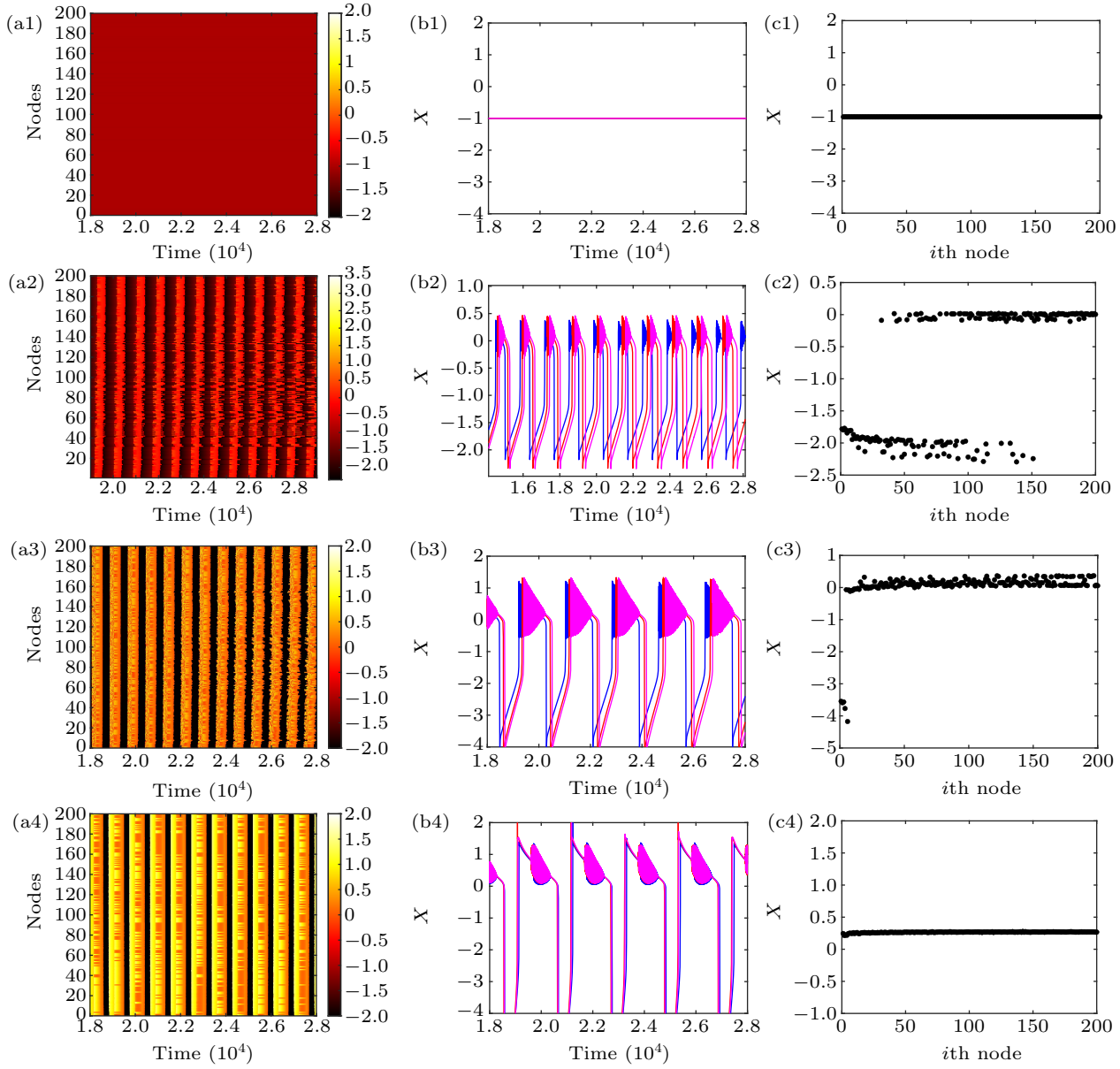


Fig. 5. Dynamical behaviors of the neural network for memristor initial values −3, −1, 1, and 2: (a1)–(a4) spatiotemporal patterns, (b1)–(b4) time series of the 1st (blue), 100th (red), and 200th (magenta) neurons, (c1)–(c4) instantaneous node state diagrams.

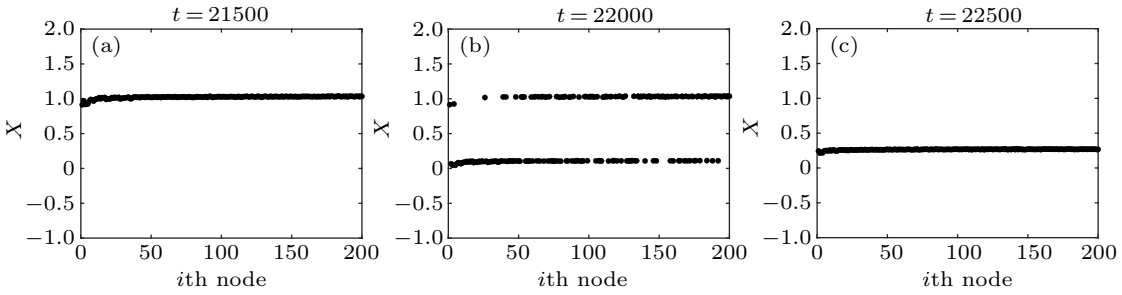


Fig. 6. Node instantaneous state diagrams of the neural network at a memristor initial value of 2.

3.2. Effect of electromagnetic induction intensity on neural network

Furthermore, this study also demonstrates that electromagnetic induction intensity plays a critical role in shaping the firing patterns of the neural network. Simulation results indicate that appropriately tuning the electromagnetic induction intensity can promote synchronization in the SWSFNN, which has important implications for pathological dynamics.

The analysis is performed with parameters set to $\alpha = 4$, $b = 0.001$, $\delta = -1$, and $k = 0.001$. The initial memristor value is set to 1, and the initial values of both fast and slow neuronal variables are set to 0. The dynamical behavior of the neural

network is then examined under different electromagnetic induction intensities.

When the electromagnetic induction intensity is $w = 0$, i.e., there is no electromagnetic effect, Figs. 7(a1)–7(c1) show irregular spatiotemporal patterns, desynchronized firing in the time series, and disordered scattered points, indicating asynchronous behavior of the SWSFNN. However, once electromagnetic effects are introduced, the synchronization behavior changes significantly.

At $w = 0.1$, the network exhibits a chimera state, where synchronized and desynchronized dynamics coexist. As shown in Figs. 7(a2)–7(c2), the first 80 nodes display irregular spatiotemporal patterns and scattered activity, indicating asynchronous dynamics, while the remaining nodes exhibit more regular behavior, corresponding to a synchronized state.

When $w = 0.3$, Figs. 7(a3)–7(c3) reveal uniform spatiotemporal patterns, synchronized firing in the time series, and concentrated state distributions, indicating significantly enhanced synchronization in the SWSFNN. These results demonstrate that electromagnetic induction facilitates synchronization in the network.

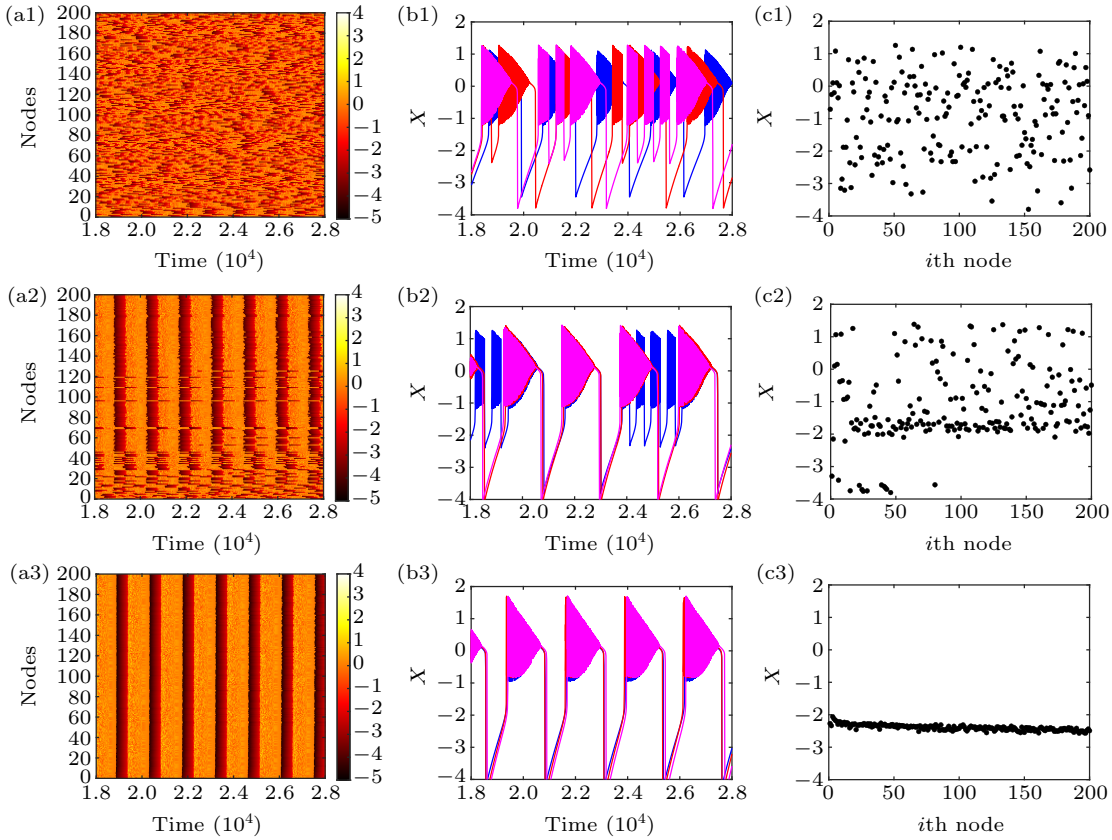


Fig. 7. Dynamical behaviors of the neural network under electromagnetic induction intensities $w = 0$, 0.1, and 0.3: (a1)–(a3) spatiotemporal patterns. (b1)–(b3) time series of the 1st (blue), 100th (red), and 200th (magenta) neurons. (c1)–(c3) instantaneous state diagrams.

4. Conclusion

This paper presents a neural network model that incorporates both small-world and scale-free properties, where discrete memristors are employed to model the influence of external electromagnetic fields. The dynamical behaviors of the SWSFNN under electromagnetic effects are systematically investigated. Numerical simulations reveal that the initial value of the memristor not only influences neuronal firing patterns but also plays a crucial role in regulating network synchronization states.

Notably, a "synchronization–cluster synchronization–synchronization" transition is observed under constant system parameters. This result indicates that neural networks can exhibit complex synchronous dynamics even in the absence of parameter variation, providing important theoretical insights into nonlinear dynamical mechanisms, synchronization–desynchronization transitions, and information processing in neural systems.

Furthermore, it is demonstrated that electromagnetic induction intensity enhances synchronization in the SWSFNN. These findings provide both theoretical foundations and practical implications for neural control and dynamical analysis of neural systems under electromagnetic effects.

Acknowledgments

This work was supported by the Key Research and Development Plan of Hunan Province (Grant No. 2026QK3023) and the Natural Science Foundation Project of Hunan Province

(Grant Nos. 2026JJ50521 and 2026JJ81304).

References

[1] Chua L 1971 *IEEE Trans. Circuit Theory* **18** 507

[2] Strukov D B, Snider G S, Stewart D R and Williams R S 2008 *Nature* **453** 80

[3] Chen W, Song L, Wang S, Zhang Z, Wang G, Hu G and Gao S 2023 *Adv. Electron. Mater.* **9** 2200833

[4] He S, Peng Y, Wang H, Li C and Ma M 2025 *Nonlinear Dyn.* **113** 28119

[5] Deng Q, Wang C, Sun Y, Deng Z and Yang G 2025 *IEEE Trans. Circuits Syst. I: Regul. Pap.* **72** 300

[6] Deng Q, Wang C, Sun Y and Yang G 2025 *IEEE Trans. Cybern.* **55** 3926

[7] Lai Q and Qin M 2025 *IEEE Trans. Cybern.* **56** 557

[8] Sun J, Yang J, Wang Y and Wang Y 2025 *IEEE Internet Things J.* **12** 28598

[9] Yu F, Kong X, Yao W, Zhang J, Cai S, Lin H and Jin J 2024 *Chaos Solitons Fractals* **179** 114440

[10] Ma J 2025 *Nonlinear Dyn.* **113** 25365

[11] Xie Y, Ye Z, Wang X, Jia Y, Hu X and Li X 2025 *Chaos Solitons Fractals* **195** 116325

[12] Bao H, Hu A, Liu W and Bao B 2020 *IEEE Trans. Neural Netw. Learn. Syst.* **31** 502

[13] He S, Yu F, Guo R, Zheng M, Tang T, Jin J and Wang C 2025 *Fractal Fract.* **9** 561

[14] Bao H, Hua Z, Li H, Chen M and Bao B 2021 *IEEE Trans. Circuits Syst. I, Reg. Papers* **68** 4534

[15] Li K, Bao H, Li H, Ma J, Hua Z and Bao B 2022 *IEEE Trans. Ind. Informat.* **18** 1726

[16] Bao H, Fan J, Hua Z, Xu Q and Bao B 2025 *IEEE Internet Things J.* **12** 31843

[17] Bao H, Xi M, Tang H, Zhang X, Xu Q and Bao B 2025 *IEEE Trans. Ind. Informat.* **21** 1862

[18] Truccolo W, Donoghue J A, Hochberg L R, Eskandar E N, Madsen J R, Anderson W S, Brown E N, Halgren E and Cash S S 2011 *Nat. Neurosci.* **14** 635

[19] Oswal A, Brown P and Litvak V 2013 *Curr. Opin. Neurol.* **26** 662

[20] Uhlhaas P J and Singer W 2006 *Neuron* **52** 155

[21] Uhlhaas P J and Singer W 2010 *Nat. Rev. Neurosci.* **11** 100

[22] Muni S S, Fatoyinbo H O and Ghosh I 2022 *Int. J. Bifurcation Chaos* **32** 2230020

[23] Tang Z, Wang H, Zhu W and Sun K 2025 *Chaos Solitons Fractals* **192** 116012

[24] Watts D J and Strogatz S H 1998 *Nature* **393** 440

[25] Barabási A L and Albert R 1999 *Science* **286** 509

[26] Ma M, Yuan Z, Zhao X 2026 *Nonlinear Dyn.* **114** 275

[27] Wang M, Hou Z and Xin H 2006 *ChemPhysChem* **7** 579

[28] Batista C A S, Batista A M, de Pontes J C A, Lopes S R and Viana R L 2009 *Chaos Solitons Fractals* **41** 2220

[29] Hao Y, Gong Y, Wang L, Ma X and Yang C 2011 *Chaos Solitons Fractals* **44** 260

[30] Yao Z, Sun K and Wang H 2024 *Physica A* **639** 129673

[31] Yuan Z, Wu Y, Ou C, Zhong P, Zhao X and Ma M 2025 *Chin. J. Phys.* **94** 108

[32] Deng W and Ma M 2024 *Chin. J. Phys.* **91** 966

[33] He Y, Chen Z J and Evans A C 2007 *Cereb. Cortex* **17** 2407

[34] Lei X, Wang Y, Yuan H and Chen A 2015 *Brain Topogr.* **28** 292

[35] Bassett D S and Bullmore E 2006 *Neuroscientist* **12** 512

[36] Guo L, Liu D, Wu Y and Xu G 2023 *Neurocomputing* **529** 113

[37] Li Z, Guo Z, Wang M and Ma M 2021 *AEU-Int. J. Electron. Commun.* **142** 153995

[38] Barrat A, Barthélemy M and Vespignani A 2004 *Phys. Rev. Lett.* **92** 228701

[39] Wang D and Jin X 2012 *Acta Phys. Sin.* **61** 228901 (in Chinese)

[40] Hu X, Wu Y, Ding Q, Xie Y, Ye Z and Jia Y 2024 *Phys. D* **460** 134091

[41] Xie Y, Li X, Wang X, Ye Z, Hu X, Hu Y and Jia Y 2025 *Nonlinear Dyn.* **113** 12099

[42] Rulkov N F 2001 *Phys. Rev. Lett.* **86** 183